Thermal Balance Modulation of Switching Devices for Hybrid-Clamped Three-Level Full-Bridge LLC Resonant Converter

Junjie Qin, Zongjian Li, *Member, IEEE*, Zhixing He, *Member, IEEE*, Zhijie Weng, Renfeng Guan, *Member, IEEE*, Zhengyan Li, Qianming Xu, *Member, IEEE*, Hongliang Wang, *Senior Member, IEEE*, and Yandong Chen, *Senior Member, IEEE*

***Abstract*—The hybrid-clamped three-level full-bridge *LLC* resonant converter is widely employed in subway power systems and ship-integrated power systems due to its notable attributes of soft switching and low input voltage requirements for the switching devices. Nonetheless, the existing wide voltage range modulation modes suffer from thermal imbalances in switching devices, posing limitations on their application in high-power scenarios. In order to address these issues, the three modulation modes optimized for thermal balance are proposed by analyzing the conditions for achieving soft-switching and thermal equalization. When integrated with the original modulation modes, these optimized modes effectively balance the conduction loss in the switching devices and achieve a wide range of voltage gain. Moreover, the proposed modulation transition method facilitates swift and efficient transitions between modulation modes, while minimizing the impact on voltage and current caused by the transition process. The experimental prototype with 1.5 kW power level and 125 V-1 kV input voltage range is built to verify thermal balance effect of switching devices under the proposed modulation mode and performance of the proposed modulation transition method.**

***Index Terms*—Heat balance optimization, *LLC* resonant converter, modulation transition, multilevel dc–dc converter.**

I. Introduction

THE isolated dc–dc power supplies with a wide voltage regulation range are widely used in photovoltaic systems, high-speed train and subway power systems, ship power systems, aerospace power systems, and so on [1], [2], [3], [4], [5]. Full-bridge or half-bridge *LLC* resonant converter have become the primary choice for isolating dc–dc due to their simple structure, high efficiency, and full-range soft-switching capabilities. The input voltage of converter has been increasing in recent years. However, the commonly used full-bridge or half-bridge topologies lead to high voltage stress on switching devices [6], [7], [8], [9], [10], [11].

Three-level converters comprise various topologies, most of which can effectively reduce the voltage stress on switching devices, making them more suitable for applications with high input voltage. The serial-half-bridge topology, which consists of two half-bridge circuits connected in series, is currently one of the simplest three-level options [12], [13], [14]. Nevertheless, the neutral-point voltage of the serial-half-bridge topology will diverge if there is time delay of control and driver circuits. Therefore, the neutral-point voltage balance control is necessary to maintain the voltage stress balance of switching devices, resulting in an increased complexity of control [15], [16], [17]. Compared with the other three-level half-bridge topologies, the hybrid-clamped three-level half-bridge topology combines the advantages of both diode-clamped and flying-capacitor three-level half-bridge topologies, allowing for maintaining devices stress balance without control. A wide voltage gain range can be achieved with the hybrid-clamped three-level half-bridge converter through the combination of different modulation modes [18], [19]. However, the current stress on the switching devices of the half-bridge converter is excessively high in high-power applications, which hinder its utilization in such scenarios.

The multilevel full-bridge inverter is capable of outputting various levels while reducing the current stress on the switching devices. When combined with the *LLC* resonator, it can achieve a variety of modulation modes. In the diode-clamped three-level full-bridge *LLC* resonant converter, a flexible variable-mode control for wide gain range application is proposed in [20]. Similarly, in the diode-clamped four-level full-bridge *LLC* resonant converter, a pulse amplitude modulation operating at the resonant frequency is proposed in [21]. Nevertheless, these two modulations increase the analytical complexity and reduce the efficiency of the converter because some switching devices are turned OFF near the peak current. In contrast, the two-level modulation mode is more suitable for *LLC* resonant converter. Three two-level modulation modes for serial flying-capacitor three-level half-bridge *LLC* resonant converter are proposed in [22]. The amplitude of the square wave level in the input

Manuscript received 15 October 2023; revised 5 January 2024 and 6 February 2024; accepted 7 February 2024. Date of publication 21 February 2024; date of current version 20 March 2024. This work was supported in part by the National Natural Science Foundation of China under Grant 52107193 and in part by the National Key Research and Development Program of China under Grant 2022YFB2404800. Recommended for publication by Associate Editor F.J. Azcondo. *(Corresponding author: Zongjian Li.)*

The authors are with the College of Electrical and Information Engineering, Hunan University, Changsha 410082, China (e-mail: qin12138@hnu.edu.cn; lzjq1@hnu.edu.cn; hezhixing@hnu.edu.cn; wzj80865@hnu.edu.cn; grf@hnu.edu.cn; lzy1494164391@hnu.edu.cn; xqm@hnu.edu.cn; wanghl123@hnu.edu.cn; yandong_chen@hnu.edu.cn).

Color versions of one or more figures in this article are available at https://doi.org/10.1109/TPEL.2024.3368089.

Digital Object Identifier 10.1109/TPEL.2024.3368089

resonator exhibits significant variations under different modulation modes, enabling a wide range of gain modulation through the combination of various modulation modes. However, there are noticeable differences in the conduction time of switching devices in certain modulation modes, which can result in imbalanced losses for these switching devices and affect their application in high-power scenarios. Moreover, the transition method between different modulation modes will affect the output characteristics of the converter.

There are differences in voltage and current states among modulation modes, so direct transition may result in significant current overshoot and output voltage variation. The transition method proposed in [23] involves gradually changing the duty cycle to transition between modulation modes in the *LLC* resonant converter. The frequency is adjusted dynamically throughout the conversion process, ensuring a smooth output voltage. Nevertheless, the mode transition time is long, and the switching devices cannot achieve zero voltage switching (ZVS) during the transition process. In [24], a transition method is proposed in which all switching devices are first turned OFF and then start at highest frequency during the transition process, but the turn-OFF period of the converter results in a significant voltage drop under full load. It is proposed that increasing the switching frequency of modulation mode after transition can reduce the current overshoot caused by direct transition in [25]. Furthermore, a modulation transition method based on trajectory control for *LLC* resonant converter is proposed in [12]. However, the method requires that the two state trajectories before and after the transformation to coincide, and the calculation process is complex.

To address these issues, this article proposes the heat balance optimization modulation mode for hybrid-clamped three-level full-bridge *LLC* resonant converter by analyzing its characteristics. Furthermore, a modulation transition method is proposed to minimize the impact on voltage and current caused by the transition process, which can be easily implemented. The rest of this article is organized as follows. In Section II, the hybrid-clamped three-level full-bridge *LLC* resonant converter topology and normal modulation modes are analyzed. Section III describes the conditions of heat balance optimization and soft switching. In Section IV, three modulation modes after heat balance optimization are proposed based on the conditions. In Section V, a modulation transition method is presented, which can realize the transition between modulation modes quickly and effectively. In Section VI, a prototype with 1.5 kW power level and 125 V-1 kV input voltage range is built to validate the modulation mode and transition method. Finally, Section VII concludes this article.

II. Topology and Normal Modulation Modes

Fig. 1 shows the topology of hybrid-clamped three-level full-bridge *LLC* resonant converter. It consists of a hybrid-clamped three-level full-bridge inverter, an *LLC* resonant tank, a transformer T, and a rectifier connecting to the load. Series resonant inductor L_r, parallel resonant inductor L_m, and series resonant capacitor C_r form the *LLC* resonant tank. The reference directions of resonant current i_{Lr}, transformer magnetizing current i_{Lm}, and resonant capacitor voltage v_{Cr} are also illustrated in Fig. 1. The flying capacitor in the topology is larger, and the operating characteristics of the topology are more similar to the flying-capacitor three-level topology.

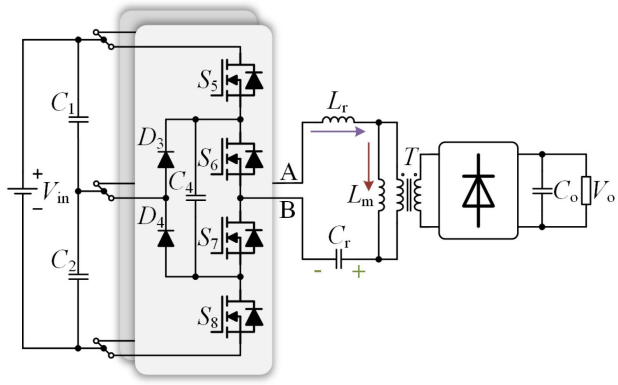

Fig. 1. Hybrid-clamped three-level full-bridge *LLC* resonant converter topology.

The hybrid-clamped three-level full-bridge inverter is capable of outputting five levels (V_{in}, $-V_{in}$, $V_{in}/2$, $-V_{in}/2$, and 0), and various types of modulation can be achieved by combining different levels. However, the application of multilevel modulation in the resonant converter leads to the significant turn-OFF losses due to partial switching devices being turned OFF near the peak current. Meanwhile, the implementation of multilevel modulation may result in the loss of ZVS for certain switching devices. In contrast, two-level modulation fully utilized the characteristics of resonant converter while employing simpler modulation methods.

Li et al. [22] proposed three modulation methods for the serial flying-capacitor three-level half-bridge *LLC* resonant converter, which are also applicable to the hybrid-clamped three-level full-bridge *LLC* resonant converter. The ratio of the modulation square wave's half to the input voltage is utilized in the subsequent discussion to effectively illustrate the characteristics of each modulation mode. The three modulation modes can be described as the unity gain modulation mode, the 1/2 gain modulation mode, and the 1/4 gain modulation mode. Furthermore, the 3/4 gain modulation mode and three level modulation mode are proposed by analyzing the hybrid-clamed three-level full-bridge inverter for all output levels. All modulation modes are depicted in Figs. 2 and 3.

The loss of switching devices is mainly composed of conduction loss, turn-ON loss, and turn-OFF loss. For the MOSFET switching device, the turn-ON loss of the device will be significantly greater than the turn-OFF loss due to its large junction capacitance. The *LLC* resonant converter can achieve ZVS, which means that the switching devices experience no turn-ON loss. The loss analysis of the *LLC* resonant converter in [26] indicates that the conduction loss of the MOSFET reaches a high level of 83.88%, even though the output current is only 0.6 times the rated current. The diagram is depicted in Fig. 4.

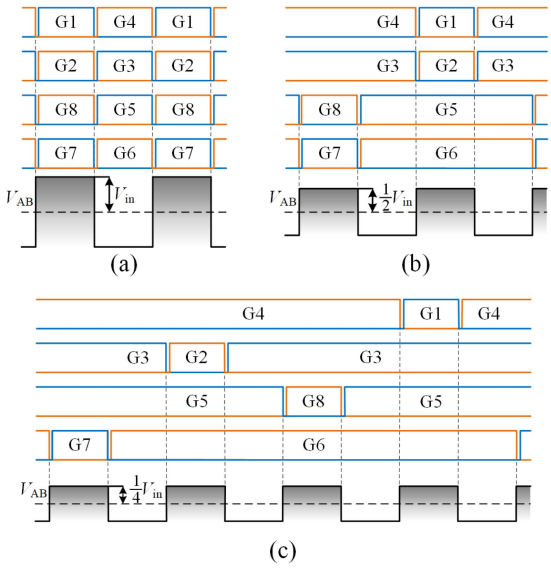

Fig. 2. Driving waveforms of the three gain modulation modes proposed in [22]. (a) Driving waveform in unity gain modulation mode. (b) Driving waveform in 1/2 gain modulation mode. (c) Driving waveform in 1/4 gain modulation mode.

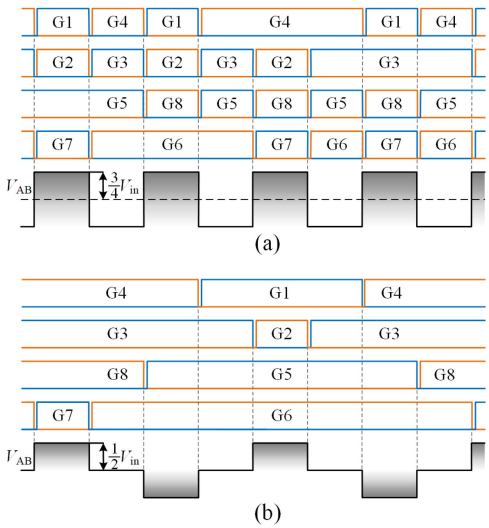

Fig. 3. Two modulation modes driving waveforms. (a) Driving waveform in 3/4 gain modulation mode. (b) Driving waveform in three-level modulation mode.

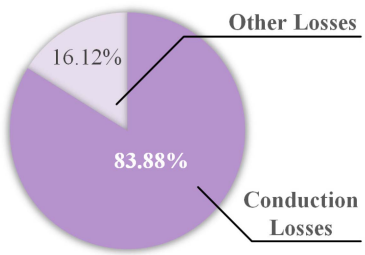

Fig. 4. Composition of MOSFET loss in *LLC* resonant converter when $I_{load} = 0.6I_{nom}$ [26].

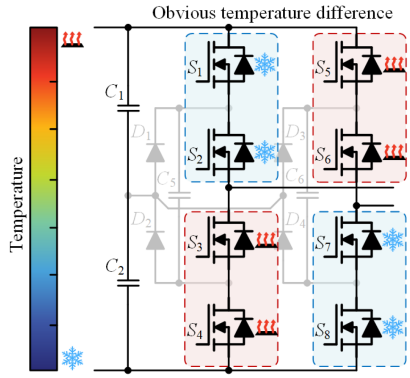

Fig. 5. Heating of the switching devices in these modulation modes.

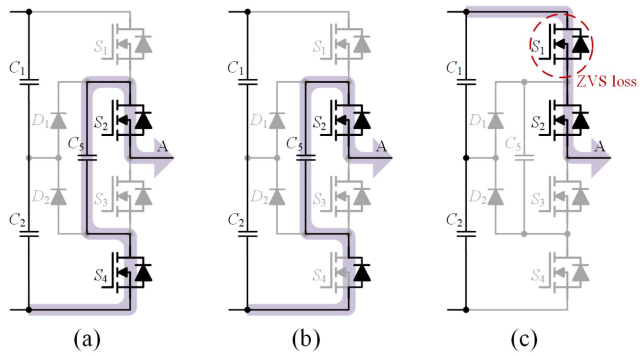

Fig. 6. State switching process of the hybrid-clamped three-level half-bridge inverter. (a) State before switching. (b) State during switching. (c) State after switching.

The conduction time of some switching devices exhibits significant differences in the 1/2 gain modulation mode, the 1/4 gain modulation mode, and the three-level modulation mode. The heating of the switching devices in these modulation modes is illustrated in Fig. 5. In these modulation modes, the heating of switching devices is uneven, which limits their application in medium and high-power occasions.

III. Condition of Soft-Switching and Thermal Equalization

To simplify the analysis difficulty, the condition for soft-switching and thermal equalization of hybrid-clamped three-level half-bridge switching devices are analyzed.

A. Condition of Soft Switching

The implementation of soft-switching is not only associated with the resonant converter but also involves the state switching of the inverter. A typical state switching process is shown in Fig. 6, where the current remains in the state that flows out of the inverter. Before the state switching, switches S_2 and S_4 maintain their conducting states, which prompts the current to flow out of the inverter through them. During the dead-time of switching between the two states, switch S_2 remains ON and switch S_4 is turned OFF. The antiparallel diode of switch S_4 is conducting, and the current path of the inverter remains unchanged. Since

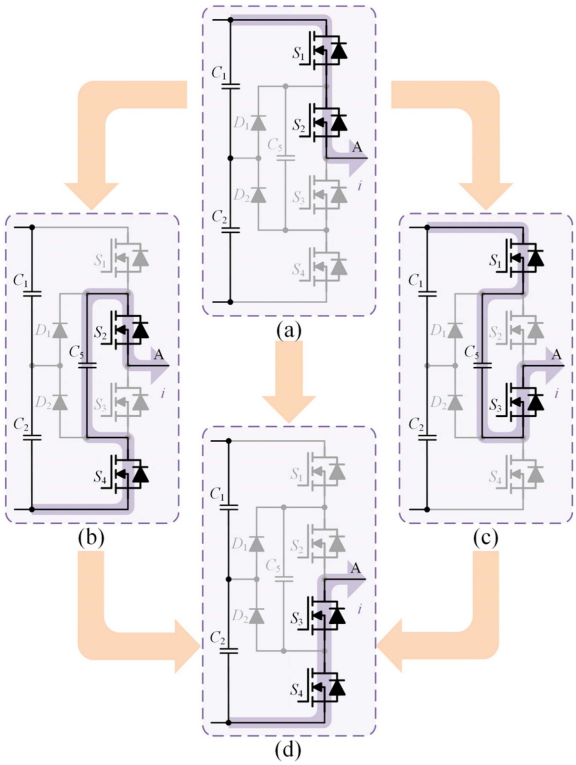

Fig. 7. Four states of the hybrid-clamped three-level half-bridge operation. (a) State I. (b) State II. (c) State III. (d) State IV.

the current does not flow through the antiparallel diode of switch S_1, the charge on the junction capacitor is not discharged when switch S_1 is turned ON. Consequently, switch S_1 is turned ON without ZVS.

By analyzing the four states of the inverter when current flows out, the state switching satisfying the ZVS condition can be obtained, which is represented by the orange arrow in Fig. 7. The arrow in Fig. 7 leads to the following conclusion: Only state switching that results in a decrease in the output potential of the inverter can achieve ZVS when current flows out it. Accordingly, when the current is reversed, the arrow of the state switching should also be reversed.

B. Condition of Thermal Equalization

The conduction loss constitutes the main portion of the total power dissipation in the switching device under full load condition. The thermal unevenness occurs in switching devices when the duty cycle is inconsistent; and the greater the difference in duty cycle, the more severe the thermal unevenness becomes.

The four operating states of the hybrid-clamped three-level half-bridge inverter are depicted in Fig. 7. To maintain voltage equalization on the flying capacitor, the state time in Fig. 7(b), and the state time in Fig. 7(c) should be consistent when the converter operates in two-level modulation mode. Denote by t_x ($x = a$, b, c or d) duration of state x in one switching cycle. The switching period of the converter is T, then t_b and t_c can be expressed as

$$t_b = t_c = \frac{T - t_a - t_d}{2}. \tag{1}$$

Ignoring the dead time, the hybrid-clamped three-level half-bridge inverter must be in one of its four operating states. Therefore, the half bridge output voltage V_A can be expressed as follows:

$$V_A = \frac{t_a}{T}V_{\text{in}} + \frac{t_b + t_c}{T}\frac{V_{\text{in}}}{2} + \frac{t_d}{T}\cdot 0 = \frac{t_a - t_d}{2T}V_{\text{in}} + \frac{V_{\text{in}}}{2}. \tag{2}$$

According to the switching conditions of the half bridge, the duty cycle of each switching devices can be expressed as follows:

$$\begin{aligned} d(G_1) &= \frac{t_a + t_b}{T},\ d(G_2) = \frac{t_a + t_c}{T} \\ d(G_3) &= \frac{t_b + t_d}{T},\ d(G_4) = \frac{t_c + t_d}{T}. \end{aligned} \tag{3}$$

By substituting (1) and (2) into (3), it can be expressed as follows:

$$\begin{aligned} d(G_1) = d(G_2) &= \frac{1}{2} + \frac{t_a - t_b}{2T} = \frac{V_A}{V_{\text{in}}} \\ d(G_3) = d(G_4) &= \frac{1}{2} - \frac{t_a - t_b}{2T} = 1 - \frac{V_A}{V_{\text{in}}}. \end{aligned} \tag{4}$$

The relationship between the duty cycle of the switching devices and the average output voltage of the inverter is expressed in (4). The duty cycle of the switching device affects its conduction time, which in turn influences its conduction loss. The duty cycle difference of switching devices becomes smaller as the average output voltage of the inverter approaches half of input voltage. The switching devices can achieve thermal equalization when the average output voltage of the inverter is half of input voltage. Additionally, the dc component of the resonant capacitor voltage becomes zero when the average output voltage of both inverter bridges reaches zero.

IV. Modulation Mode After Heat Balance Optimization

A. 1/2 Gian Modulation After Heat Balance Optimization

A hybrid-clamped three-level half-bridge inverter can output three levels (V_{in}, $V_{\text{in}}/2$, and 0). The addition of intermediate level states to the modulation mode can result in an average output voltage that is approximately half of the input voltage. When outputting unidirectional current, it is necessary to ensure that the modulation mode includes both intermediate level output states. Otherwise, the voltage on the flying capacitor will diverge. Each driving waveform in 1/2 gain modulation mode after heat balance optimization is shown in Fig. 8. Each operating state diagram of 1/2 gain modulation mode after heat balance optimization is shown in Fig. 9.

B. Three-Level Modulation After Heat Balance Optimization

The converter will enter the three-level modulation mode once the frequency of 1/2 gain modulation mode after heat balance

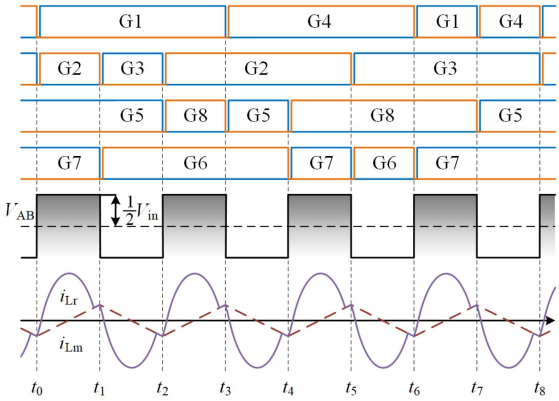

Fig. 8. Driving waveform in 1/2 gain modulation mode after heat balance optimization.

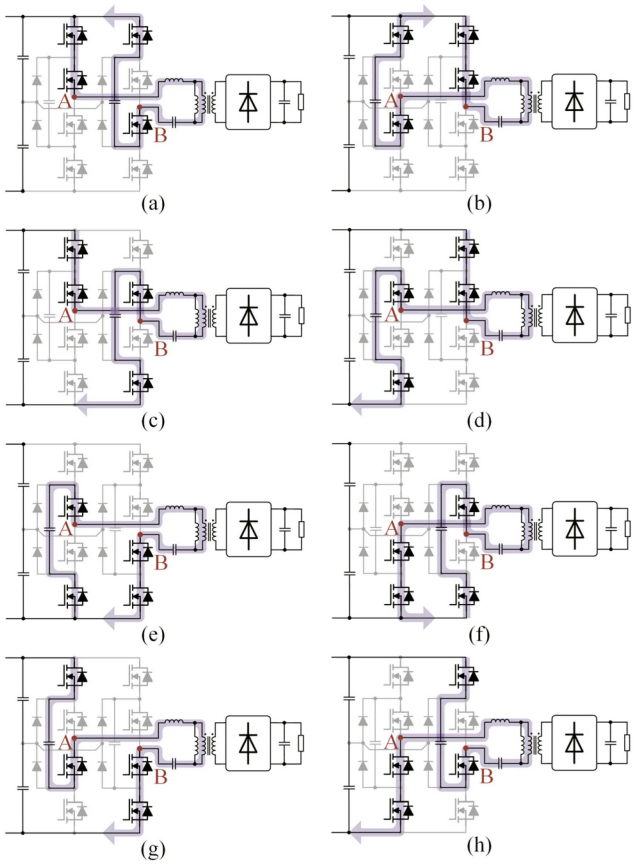

Fig. 9. Each operating state diagram of hybrid-clamped three-level Full-bridge *LLC* resonant converter in 1/2 gain modulation mode after heat balance optimization. (a) Stage t_0–t_1. (b) Stage t_1–t_2. (c) Stage t_2–t_3. (d) Stage t_3–t_4. (e) Stage t_4–t_5. (f) Stage t_5–t_6. (g) Stage t_6–t_7. (h) Stage t_7–t_8.

optimization reaches its maximum value. The three-level modulation mode can be achieved by incorporating the states of outputting zero level into the 1/2 gain modulation mode. However, the hybrid-clamped three-level full-bridge inverter is capable of achieving a zero-voltage state among its six states. It is difficult to realize the symmetrical three-level modulation mode under the condition of soft switching, as it requires introducing eight zero-level states in modulation cycle. In contrast, the asymmetric three level modulation mode only needs to add four zero-level

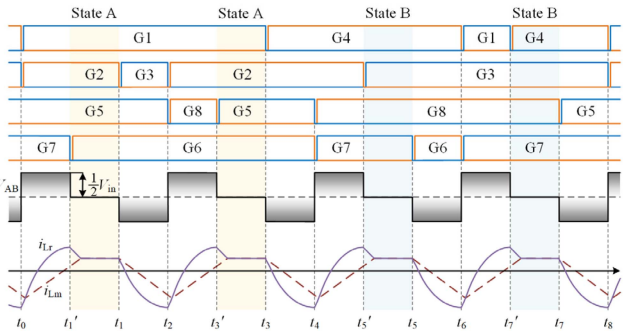

Fig. 10. Driving waveform in three-level modulation mode after heat balance optimization.

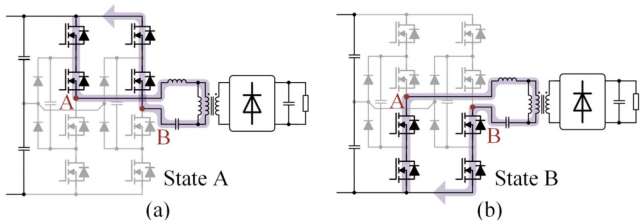

Fig. 11. Two additional states in the three-level modulation mode after heat balance optimization. (a) State A. (b) State B.

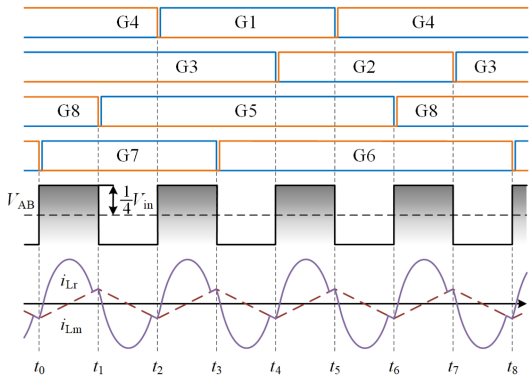

Fig. 12. Driving waveform in 1/4 gain modulation mode after heat balance optimization.

states in the modulation cycle, which significantly reduces the implementation difficulty. Each driving waveform in three-level modulation mode after heat balance optimization is shown in Fig. 10. The two additional states are shown in Fig. 11.

C. 1/4 Gian Modulation After Heat Balance Optimization

Similar to the 1/2 gain modulation mode, the 1/4 gain modulation mode can be optimized for thermal balance by increasing the duration of the output intermediate level state. Each driving waveform in 1/4 gain modulation mode after heat balance optimization is shown in Fig. 12. Each operating state diagram of 1/4 gain modulation mode after heat balance optimization is shown in Fig. 13. After optimizing heat balance, the 1/4 gain modulation mode can maintain its advantage of reducing turn-OFF losses

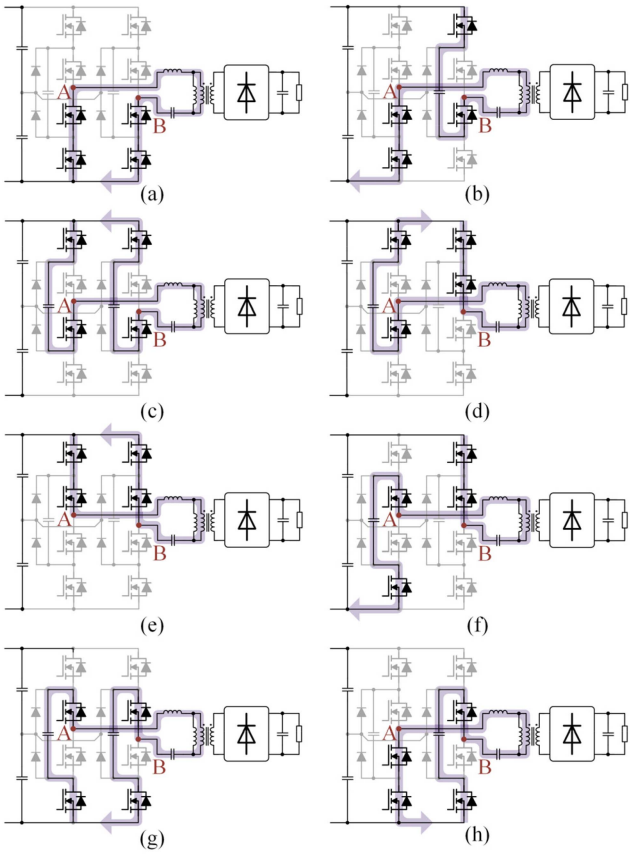

Fig. 13. Each operating state diagram of hybrid-clamped three-level Full-bridge *LLC* resonant converter in 1/4 gain modulation mode after heat balance optimization. (a) Stage t_0–t_1. (b) Stage t_1–t_2. (c) Stage t_2–t_3. (d) Stage t_3–t_4. (e) Stage t_4–t_5. (f) Stage t_5–t_6. (g) Stage t_6–t_7. (h) Stage t_7–t_8.

for switching devices by having fewer switching times in the modulation period.

V. Modulation Transition Method

Apart from the transition between the 1/2 gain modulation mode and the three-level modulation mode, it is not possible to achieve a natural and fast transition between other modulation modes due to their different driving waveforms. An unreasonable transition method may result in significant voltage and current impacts. The factors that influence voltage and current impacts are mainly divided into two parts: one is the difference in trajectory radius before and after the transition, and the other is the inconsistent gain before and after the transition. Furthermore, irrational choices of transition moments can also lead to impacts.

A. Modulation Transition Moment

The trajectories of the 1/2 gain modulation mode and the 3/4 modulation mode for the modulation transition under ideal conditions are plotted in Fig. 14. The transition of the remaining modulation modes is similar. The input voltage, output voltage, and output power of the converter are considered to remain unchanged before and after the transition since the transition process occurs very rapidly. The state trajectory of the 1/2 gain modulation mode contains two circle centers (O2, O3), which

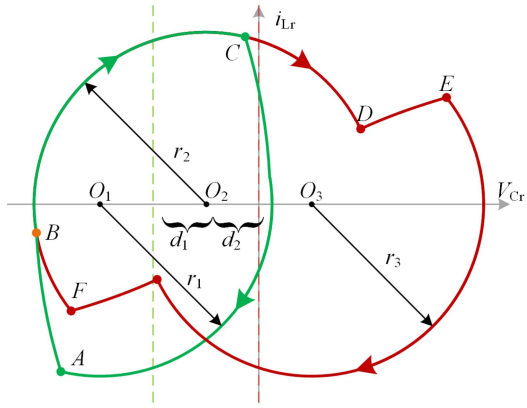

Fig. 14. Trajectories of the 1/2 gain modulation mode (red) and the 3/4 gain modulation mode (green) for the modulation transition.

are determined by the two-level states of the input resonator. Similarly, the 3/4 gain modulation mode also includes two circle centers. Since the same level state is included in both modulation mode, O2 is the common center of the two trajectories. The common center of the circle causes the two trajectories to coincide between points B and C. The 3/4 gain modulation mode changes the resonator input level state at either point A or point C on the trajectory diagram. Under ideal conditions, the transition from 3/4 gain modulation mode to 1/2 gain modulation mode at point A is completed immediately without any transients. Furthermore, fast transition can be easily achieved by switching between two modulation modes at the beginning of the same output level state.

B. Impact of Trajectory Radius Difference

The trajectories depicted in Fig. 14 represent an ideal situation. However, the trajectories of the two states may not perfectly coincide. In more general cases, the mode transition may result in a certain voltage and current overshoot. As an example, the waveform of modulation transition from 3/4 gain modulation mode to 1/2 gain modulation mode is illustrated in Fig. 15. The switching frequency is f_1 in the 3/4 gain modulation mode and f_2 in the 1/2 gain modulation mode, while the output voltage of both modes remains the same. The ac component of the voltage across the serial resonant capacitor is represented as ΔV_{Cr}. At time t_{x}, the driving signal is switched from 3/4 gain modulation mode to 1/2 gain modulation mode. At time t_1, the series resonant inductor current and the ac component of the series resonant capacitor voltage can be expressed as

$$i_{Lr}(t_1) = -\frac{nV_o}{4L_m f_1}$$
$$\Delta V_{Cr}(t_1) = -\frac{I_o}{4nC_r f_1}. \tag{5}$$

In Fig. 14, d_1 is defined as the distance between O_2 and the average voltage of the resonant capacitor before transition, while d_2 represents the distance between O_2 and the average voltage of the resonant capacitor after transition. By normalizing all voltages with the voltage factor nV_{o}, and all currents with the

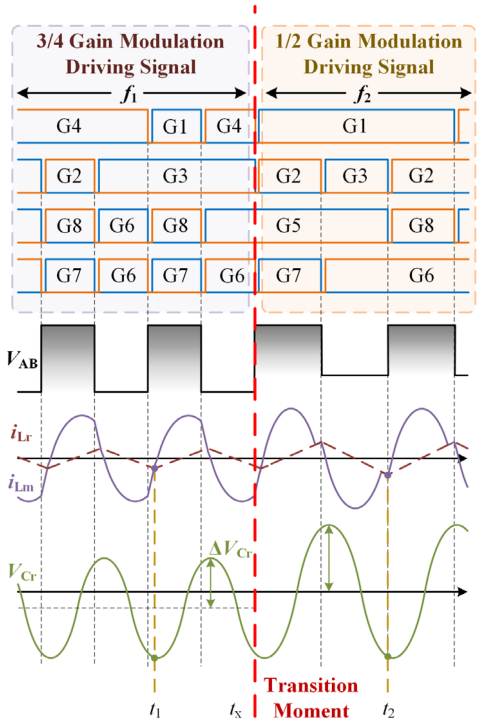

Fig. 15. Waveform of modulation transition from 3/4 gain modulation mode to 1/2 gain modulation mode.

current factor nV_o/Z_0, the following expressions are derived:

$$r_2(t_1) = \sqrt{\left(\frac{Z_o}{4L_m f_1}\right)^2 + \left(\frac{I_o}{4nV_oC_r f_1} + d_1\right)^2}. \quad (6)$$

Assuming that the circuit has been operating stably at time t_2, the radius r_2 can be expressed as follows:

$$r_2(t_2) = \sqrt{\left(\frac{Z_o}{4L_m f_2}\right)^2 + \left(\frac{I_o}{4nV_oC_r f_2} - d_2\right)^2}. \quad (7)$$

By ignoring distances d_1 and d_2, and combining (4) and (5), the following can be derived:

$$\frac{r_2(t_2)}{r_2(t_1)} < \frac{f_1}{f_2}. \quad (8)$$

Δr_2 represents the difference in radius before and after the transition, while $\Delta r_2{}^*$ represents the difference between the radius during the transition and the radius after reaching steady state, so

$$\Delta r_2^* < \Delta r_2 = r_2(t_2) - r_2(t_1). \quad (9)$$

The maximum value of the radius r_2 in the transition process is denoted as $r_{2\max}$, and it can be expressed as follows:

$$\frac{r_{2\max}}{r_2(t_2)} < \frac{r_2(t_2) + \Delta r_2}{r_2(t_2)} < 2 - \frac{f_2}{f_1}. \quad (10)$$

When the converter operates stably at switching frequency f_2, $i_{Lr\max}$ represents the maximum value of the resonant current and $v_{Cr\max}$ represents the maximum value of the resonant voltage. The upper limit of the impact caused by the resonant voltage

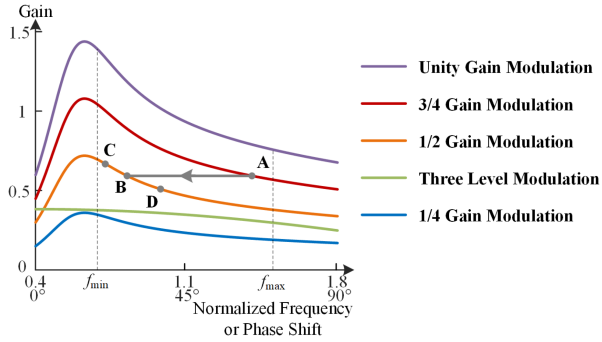

Fig. 16. Curves of gain transformation under five modulation modes.

$v_{Cr\max}{}^*$ and resonant current $i_{Lr\max}{}^*$ during the transition process can be estimated as follows:

$$i_{Lr\max}{}^* < \left(2 - \frac{f_2}{f_1}\right) i_{Lr\max}$$
$$v_{Cr\max}{}^* < \left(2 - \frac{f_2}{f_1}\right) v_{Cr\max}. \quad (11)$$

The switching frequency before and after the transition will not have a significant difference due to the operating frequency limitation of magnetic. Additionally, considering the influence of the distance d_1 and distance d_2 in Fig. 12, the overshoot of resonant voltage and resonant current during the transition process is small. When transitioning from the 1/2 gain modulation mode to the 3/4 gain modulation mode, the voltage and current impact during the transition will not exceed the voltage and current before the transition. The only difference between all the other transition is the distance d_1 and d_2, which results in the same conclusion.

C. Impact of Gain Change

Taking the example of a hybrid-clamped three-level full-bridge *LLC* resonant converter with a quality factor $Q_L = 0.5$ and an inductance ratio $L_m/L_r = 2.5$, the curves of the gain transformation with normalized frequency or phase shift angle under five modulation modes are illustrated in Fig. 16. Point A in the figure is in the 3/4 gain modulation mode, while points B, C, and D are in the 1/2 gain modulation mode. The voltage gain at point A is equivalent to that at point B, ensuring a smooth transition between the two points without any circuit impact caused by the gain transformation. The circuit operating at point C has a higher voltage gain. When the circuit switches from point A to point C, the output voltage is lower than the steady state value, and a large impact current will be generated by the circuit to charge the output capacitor. The current impact is primarily influenced by the impedance of the resonant network. If the switching frequency is close to the resonant frequency, the impedance effect of the resonant network will be reduced, resulting in a larger current impact on the circuit. When the circuit switches from point A to point D, the output voltage becomes higher than the steady state value and is primarily maintained by the output capacitor. The *LLC* resonant converter primarily operates in the three-element resonant state without

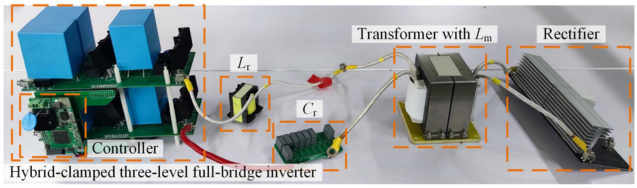

Fig. 17. Experimental prototype of the proposed converter.

TABLE I
PARAMETERS OF THE EXPERIMENTAL PROTOTYPE

Quantity	Values
Input voltage V_{in}	125 V-1kV dc
Output voltage V_o	400 V dc
Output power P_o	1.5 kW
Resonant capacitor C_r	72 nF
Resonant inductor L_r	18 μH
Magnetic inductor L_m	45 μH
Resonant frequency f_r	140 kHz
Switching frequency f	100 kHz–200 kHz
Transformer turn ratio	1:2
MOSFETs S_1-S_8	IV1Q06040T4
Secondary diodes	VS-40EPS08-Ms
Clamped diodes D_1-D_4	S10MC
Dead time	200 ns

energy output, thereby avoiding voltage and current impact during switching. When the output voltage is lower than the target value, the control circuit reduces the switching frequency in order to increase the output voltage back up to the target value. The control parameters determine the voltage and the current overshoot of the voltage regulation process. Therefore, switching from point A to point B represents the optimal strategy. Since the calculated voltage gain curve may differ from the actual voltage gain, it is advisable to choose a transition point slightly lower than point B in order to avoid the impact of voltage and current during transition.

VI. EXPERIMENTAL VERIFICATION

The *LLC* resonant converter has the advantage of soft switching for its switching devices, which allows an increase in the converter's switching frequency to 100 kHz–200 kHz. The design of high-frequency transformers is based on common design method. The transformer magnetic inductor and conversion ratio can be determined based on the normalized inductance ratio, quality factor, and actual application requirements. Similarly, the type and size of the core are selected based on the converter's switching frequency and power level. By selecting the maximum magnetic flux density, the number of turns ON the primary and secondary sides of the transformer can be determined. Finally, the diameter of the wire in the transformer is determined by selected current density.

An experimental prototype with 1.5 kW power level and 125 V – 1 kV input voltage range is built to verify the effectiveness of the proposed modulation mode and transition method. The experimental prototype is shown in Fig. 17, and the parameters of this prototype are presented in Table I.

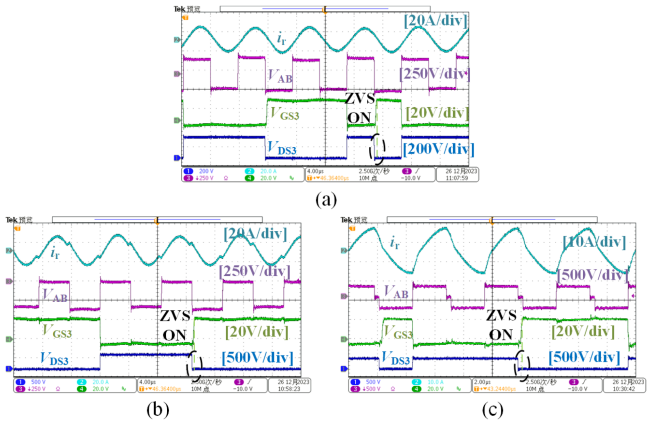

Fig. 18. Soft switching experimental waveforms of three modulation modes with optimized heat balance at full load. (a) Soft switching effect of S_3 in 1/2 gain modulation mode after heat balance optimization, with $V_{in} = 400$ V. (b) Soft switching effect of S_3 in 1/4 gain modulation mode after heat balance optimization, with $V_{in} = 700$ V. (c) Soft switching effect of S_3 in three-level modulation mode after heat balance optimization, with $V_{in} = 600$ V.

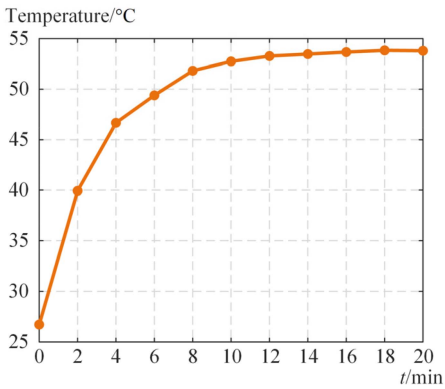

Fig. 19. Temperature rise curve of the switching devices.

A. Soft Switching Effect of Modulation Modes After Heat Balance Optimization

Fig. 18 illustrates the soft switching experimental waveforms of three modulation modes with optimized heat balance at full load. Here, i_{Lr} represents the current flowing through the serial resonant inductor, V_{GS3} represents the driving signal of the switching device S_3, V_{DS3} represents the voltage across the switching device S_3, and V_{AB} represents the input voltage of the resonator. The experimental waveforms demonstrate that the switching devices can achieve excellent soft-switching effects under three modulation modes after heat balance optimization.

B. Effect of Heat Balance Optimization

The temperature rise curve of the switching device is depicted in Fig. 19. The curve indicates that the temperature stabilizes when the operation time of the switching device reaches 20 min. Fig. 20 illustrates the temperature comparison of switching devices S_1 and S_4 before and after heat balance optimization. Before the heat balance optimization, the temperature difference between switching devices S_1 and S_4 is 15.2 °C in 1/2 gain modulation mode, 18.6 °C in three-level modulation mode, and

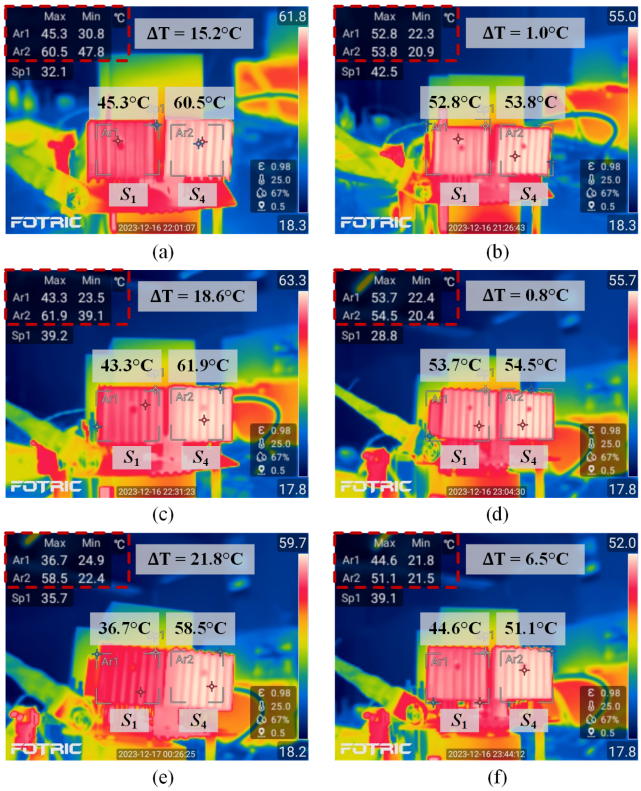

Fig. 20. Temperature difference of switching devices S_1 and S_4 before and after heat balance optimization. (a) In total, 1/2 gain modulation mode before heat balance optimization. (b) In total, 1/2 gain modulation mode after heat balance optimization. (c) Three-level modulation mode before heat balance optimization. (d) Three-level modulation mode after heat balance optimization. (e) In total, 1/4 gain modulation mode before heat balance optimization. (f) In total, 1/4 gain modulation mode after heat balance optimization.

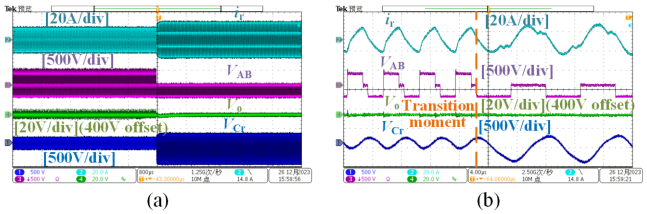

Fig. 21. Transition waveforms from three level modulation mode to 1/4 gain modulation mode at $V_{\rm in} = 650$ V with full load. (a) Whole process waveform. (b) Transient waveform.

21.8 °C in 1/4 gain modulation mode. After optimizing the thermal balance, the temperatures of switching devices S_1 and S_4 are nearly identical in 1/2 gain modulation mode and three-level modulation mode, with a difference of 6.5 °C in 1/4 gain modulation mode. Therefore, the proposed optimal modulation mode can effectively achieve heat balance in switching devices.

C. Transition Process Between Modulation Modes

Figs. 21 and 22 demonstrate the experimental waveforms of transitions between different modulation modes under full load conditions. As can be observed, the resonant voltage and current exhibit no overshoot throughout the entire switching

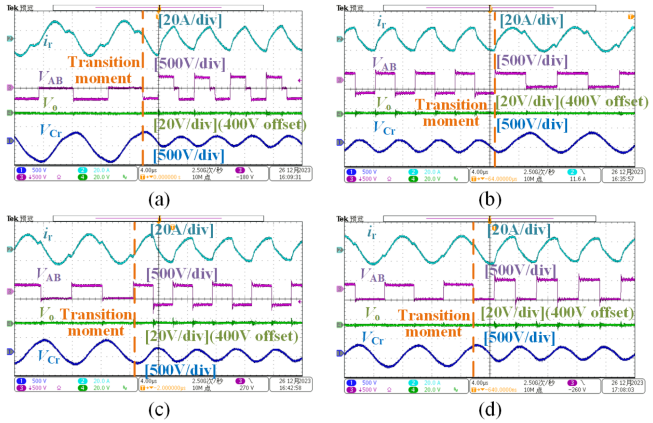

Fig. 22. Experimental waveforms of the proposed transition method. (a) In total,1/4 gain modulation mode to three level modulation mode at Vin = 650 V with full load. (b) In total, 3/4 gain modulation mode to 1/2 gain modulation mode at Vin = 350 V with full load. (c) In total, 1/2 gain modulation mode to 3/4 gain modulation mode at Vin = 350 V with full load. (d) In total, 3/4 gain modulation mode to unity gain modulation mode at Vin = 250 V with full load.

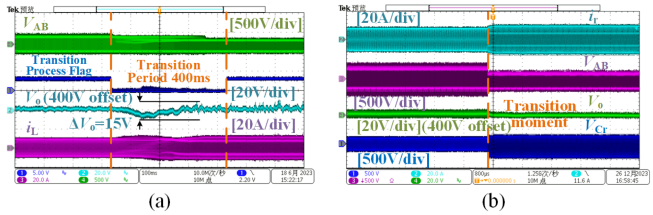

Fig. 23. Transition waveforms from unity gain modulation mode to 3/4 gain modulation mode at $V_{\rm in} = 250$ V with full load. (a) Transition by gradually changing the duty cycle and switching frequency in [23]. (b) Transition by proposed method.

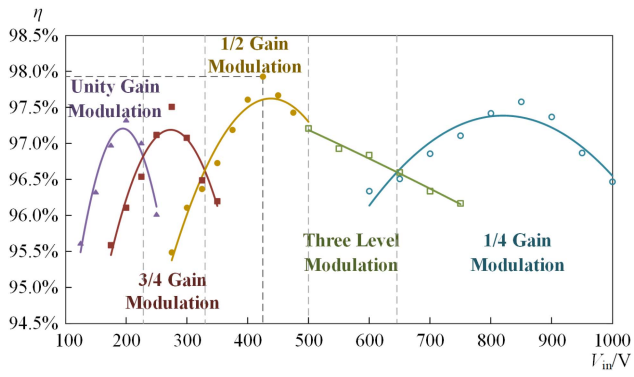

Fig. 24. Operating efficiency curves of the converter under full load conditions with various modulation modes and different input voltage.

process, and the transition between the two modes occurs instantaneously. The waveforms between [23] and the proposed transition method is shown in Fig. 23. Compared with the method in [23], the output voltage variation of the proposed method is smaller in the transition process. Therefore, the effectiveness of the proposed method has been verified.

D. Efficiency Curve

Fig. 24 illustrates the operating efficiency curves of the converter under full load conditions with various modulation modes

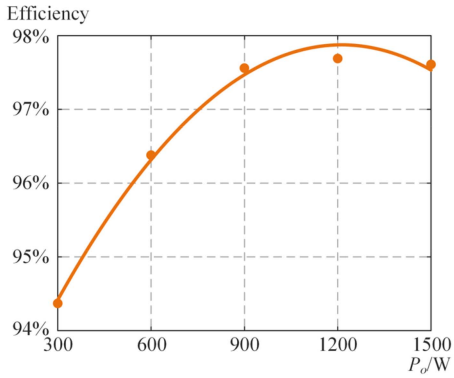

Fig. 25. Operating efficiency curves of the converter from light load to full load under 1/2 gain modulation mode when $V_{in} = 400$ V.

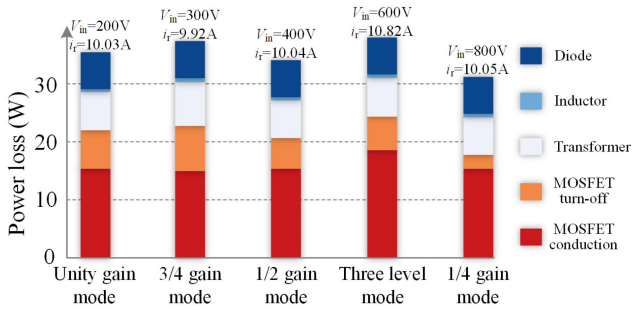

Fig. 26. Loss distribution of the converter under different modulation mode at full load.

and different input voltage. The efficiency curve of the proposed converter under different loads with the input voltage of 400 V is illustrated in Fig. 25. The loss distribution of the converter under different modulation mode at full load is shown in the Fig. 26. The operating efficiency of each modulation mode can be high within its corresponding input voltage range. By switching between each mode, the converter can maintain high efficiency under most operational conditions.

VII. Conclusion

In this article, the heat balance optimization modulation modes of hybrid-clamped three-level full-bridge *LLC* resonant converter are proposed. To validate the effectiveness of the proposed modulation modes and transition method, an experimental platform with 1.5 kW power level and 125 V-1 kV input voltage range has been established. The use of field programmable gate array (FPGA) as the controller in the prototype can effectively reduce the implementation difficulty of the proposed modulation and transition method. The optimized modulation modes achieve the thermal equilibrium in the switching devices, thereby enhancing the output power level of the converter. Additionally, the proposed transition method facilitates quick and effective transition between modulation modes. With these optimized modulation modes and transition method, the hybrid-clamped three-level full-bridge *LLC* resonant converter offers significant advantages in a wide voltage regulation range and high-power application.

References

[1] H. Luo et al., "Voltage-mode variable-frequency controlled LLC resonant power factor correction converter and its accurate numerical calculation analysis," *IEEE J. Emerg. Sel. Topics Power Electron.*, vol. 11, no. 2, pp. 1979–1994, Apr. 2023.

[2] A. Elezab, O. Zayed, A. Abuelnaga, and M. Narimani, "High efficiency LLC resonant converter with wide output range of 200–1000 V for DC-connected EVs ultra-fast charging stations," *IEEE Access*, vol. 11, pp. 33037–33048, 2023.

[3] Y.-Y. Chen et al., "1.5-MHz high-performance 380-V/12-V LLC resonant converter," in *Proc. Int. Power Electron. Conf. -Himeji Early Childhood Care Educ. Asia*, 2022, pp. 539–546.

[4] Y. Wei, Q. Luo, Z. Wang, and A. Mantooth, "Transformer secondary voltage based resonant frequency tracking for LLC converter," *IEEE Trans. Circuits Syst. II, Exp. Briefs*, vol. 68, no. 4, pp. 1243–1247, Apr. 2021.

[5] A. Rajput, N. Deshmukh, and S. Anand, "A LLC resonant converter with wide output voltage range for USB-power delivery," in *Proc. Nat. Power Electron. Conf.*, 2021, pp. 1–6.

[6] V. Sidorov, A. Chub, and D. Vinnikov, "Performance improvement of PWM control methods for voltage step-down in series resonant DC–DC converters," *Energies*, vol. 13, no. 17, pp. 1–18 2020.

[7] L. Shi, B. Liu, and S. Duan, "Burst-mode and phase-shift hybrid control method of LLC converters for wide output range applications," *IEEE Trans. Ind. Electron.*, vol. 67, no. 2, pp. 1013–1023, Feb. 2020.

[8] M. H. Ahmed, A. Nabih, F. C. Lee, and Q. Li, "Low-loss integrated inductor and transformer structure and application in regulated LLC converter for 48-V bus converter," *IEEE J. Emerg. Sel. Topics Power Electron.*, vol. 8, no. 1, pp. 589–600, Mar. 2020.

[9] F. Musavi, M. Craciun, D. S. Gautam, W. Eberle, and W. G. Dunford, "An LLC resonant DC–DC converter for wide output voltage range battery charging applications," *IEEE Trans. Power Electron.*, vol. 28, no. 12, pp. 5437–5445, Dec. 2013.

[10] G. Li, J. Xia, K. Wang, Y. Deng, X. He, and Y. Wang, "Hybrid modulation of parallel-series LLC resonant converter and phase shift full-bridge converter for a dual-output DC–DC converter," *IEEE J. Emerg. Sel. Topics Power Electron.*, vol. 7, no. 2, pp. 833–842, Jun. 2019.

[11] L. A. D. Ta, N. D. Dao, and D.-C. Lee, "High-efficiency hybrid LLC resonant converter for on-board chargers of plug-in electric vehicles," *IEEE Trans. Power Electron.*, vol. 35, no. 8, pp. 8324–8334, Aug. 2020.

[12] C. Zhang and P. Barbosa, "Modulation transition methods based on trajectory control for LLC resonant converters operating in wide input- and/or output-voltage range," *IEEE Trans. Power Electron.*, vol. 37, no. 12, pp. 14103–14114, Dec. 2022.

[13] Y. Shi, X. Wang, J. Xi, X. Gui, and X. Yang, "Wide load range ZVZCS three-level DC–DC converter with compact structure," *IEEE Trans. Power Electron.*, vol. 34, no. 6, pp. 5032–5037, Jun. 2019.

[14] C. Zhang, P. Barbosa, Z. Shen, and R. Wang, "A novel three-level phase-shift modulation for serial half bridge LLC resonant converter," in *Proc. IEEE Appl. Power Electron. Conf. Expo.*, 2021.

[15] C. Lu, W. Hu, and F. C. Lee, "Neutral-point voltage balancing methods of series-half-bridge LLC converter for solid state transformer," *IEEE Trans. Power Electron.*, vol. 36, no. 6, pp. 7060–7073, Jun. 2021.

[16] W. Liu, H. Jin, W. Yao, and Z. Lu, "An interleaved PWM method with better voltage-balancing ability for half-bridge three-level DC/DC converter," *IEEE Trans. Power Electron.*, vol. 33, no. 6, pp. 4594–4598, Jun. 2018.

[17] X. Yu, K. Jin, and Z. Liu, "Capacitor voltage control strategy for half-bridge three-level DC/DC converter," *IEEE Trans. Power Electron.*, vol. 29, no. 4, pp. 1557–1561, Apr. 2014.

[18] L. Shi et al., "Voltage autobalance characteristic analysis and clamp circuits design of hybrid-clamped three-level LLC converter," *IEEE Trans. Ind. Appl.*, vol. 55, no. 6, pp. 6026–6035, Nov./Dec. 2019.

[19] L. Zhu, Z. Sheng, F. Peng, and L. Yang, "Control strategy of half-bridge three-level LLC resonant converters with wide output voltage range," *IEEE Trans. Plasma Sci.*, vol. 50, no. 11, pp. 4381–4386, Nov. 2022.

[20] H. Tong, Z. Miao, H. Lin, W. Yao, W. Li, and Z. Lu, "A three-level LLC converter with flexible variable-mode control for wide gain range application," *IEEE Trans. Power Electron.*, vol. 38, no. 4, pp. 4503–4519, Apr. 2023.

[21] M.-S. Song and J.-B. Lee, "Pulse-amplitude-modulation full-bridge diode-clamped multilevel LLC resonant converter using multi-neighboring reference vector discontinuous PWM," *Energies*, vol. 15, no. 11, 2022, Art. no. 4045.

[22] R. T. Li, M.-F. Vancu, F. Canales, and D. Aggeler, "High performance dc-dc converter for wide voltage range operation," in *Proc. 7th Int. Power Electron. Motion Control Conf.*, 2012, vol. 2, pp. 1151–1158.
[23] M. M. Jovanovic and B. T. Irving, "On-the-fly topology-morphing control—Efficiency optimization method for LLC resonant converters operating in wide input- and/or output-voltage range," *IEEE Trans. Power Electron.*, vol. 31, no. 3, pp. 2596–2608, Mar. 2016.
[24] H. Hu, X. Fang, F. Chen, Z. J. Shen, and I. Batarseh, "A modified high-efficiency LLC converter with two transformers for wide input-voltage range applications," *IEEE Trans. Power Electron.*, vol. 28, no. 4, pp. 1946–1960, Apr. 2013.
[25] Y. Wei, Q. Luo, and H. A. Mantooth, "An LLC converter with multiple operation modes for wide voltage gain range application," *IEEE Trans. Ind. Electron.*, vol. 68, no. 11, pp. 11111–11124, Nov. 2021.
[26] E. S. Glitz and M. Ordonez, "MOSFET power loss estimation in LLC resonant converters: Time interval analysis," *IEEE Trans. Power Electron.*, vol. 34, no. 12, pp. 11964–11980, Dec. 2019.

Junjie Qin was born in Guangxi, China, in 1997. He received the B.S. degree in electrical engineering and automation from the Central South University, Changsha, China, in 2019. He is currently working toward the Ph.D. degree in electrical engineering with Hunan University, Changsha, China.

His current research interests include the medium-voltage dc system, resonant dc converter, and wide input voltage range dc–dc converter.

Zongjian Li (Member, IEEE) received the B.S. degree in electronic information engineering from the College of Engineering, Hunan Normal University, Changsha, China, in 2012, and the Ph.D. degree in electric engineering from Hunan University, Changsha, China, in 2020.

He is currently an Assistant Professor with the College of Electrical and Information Engineering, Hunan University. His research interests include silicon carbide power electronic devices and their applications in high-voltage converter applications.

Zhixing He (Member, IEEE) was born in Hunan, China, 1989. He received the B.S. degree in information science and engineering from Central South University, Changsha, China, in 2011, and the Ph.D. degree in electrical engineering from Hunan University, Changsha, China, in 2017.

He was with the Hunan University, as a Postdoctoral Researcher between 2017 and 2018. He is currently an Associate Professor with the College of Electrical and Information Engineering, Hunan University. His research interests include medium-voltage dc system, resonant dc converter, CC/CV dc/dc converters, and modular multilevel converter.

Zhijie Weng was born in Jiangxi, China, in 1999. He received the B.S. degree in electrical engineering and automation in 2021 from the Hunan University, Changsha, China, where he is currently working toward the Ph.D. degree in electrical engineering.

His current research interests include the medium-voltage dc system, resonant dc converter, and wide input voltage range dc–dc converter.

Renfeng Guan (Member, IEEE) was born in Shaanxi, China, in 1996. He received the B.S. degree in electrical engineering and automation from the Central South University, Changsha, China, in 2018. He is currently working toward the Ph.D. degree in electrical engineering with Hunan University, Changsha, China.

His research interests include the medium voltage dc system, resonant dc converter, and CC/CV dc/dc converters.

Zhengyan Li was born in Guizhou, China, in 1999. She received the B.S. degree in electrical engineering and automation from the Guizhou University, Guizhou, China, in 2022. She is currently working toward the M.S. degree in energy and power Hunan University, Changsha, China.

Her research interests include the medium-voltage dc system and resonant dc converter.

Qianming Xu (Member, IEEE) was born in Henan, China, in 1989. He received the B.S. degree in electrical engineering and automation and the Ph.D. degree in electrical engineering from Hunan University, Changsha, China, in 2012 and 2017, respectively.

Since 2019, he has been an Associate Professor with the College of Electrical and Information Engineering, Hunan University. His research interests include multilevel converter, power electronic reliability monitoring, and power quality control.

Hongliang Wang (Senior Member, IEEE) received the B.Sc. degree from Anhui University of Science and Technology, Huainan, China, in 2004, and the Ph.D. degree from Huazhong University of Science and Technology, Wuhan, China, in 2011, both in electrical engineering.

From 2013 to 2018, he was a Postdoctoral Fellow with Queen's University. Since 2018, he has been with Hunan University, Changsha, China, where he is currently a Full Professor with the College of Electrical and Information Engineering. His current research interests include multilevel topologies, high-gain topologies, parallel technologies, and virtual synchronous generator technologies for photovoltaic applications and microgrids applications, resonant converters and server power supplies, and LED drivers.

Yandong Chen (Senior Member, IEEE) was born in Hunan, China, in 1979. He received the B.S. and M.S. degrees in instrument science and technology and the Ph.D. degree in electrical engineering from Hunan University, Changsha, China, in 2003, 2006, and 2014, respectively.

He was a Professor with the College of Electrical and Information Engineering, Hunan University. His research interests include power electronics for microgrid, distributed generation, power quality, and energy storage.

Dr. Chen is a recipient of the 2014 National Technological Invention Awards of China, and the 2014 WIPO-SIPO Award for Chinese Outstanding Patented Invention. He is a Member of the IEEE Power Electronics Society.